Chapter 13

Deformation in nuclei: shapes and rapid rotation

In the discussion of Chapter 12, it became clear that in a number of mass regions, coherence in the nuclear single-particle motion results in collective effects. The most dramatic illustrations of these collective excitations is the observation of many rotational bands that extend to very high angular momentum states. At the same time, one could prove that in the bands, the nucleus seems to acquire a strongly deformed shape that is given, in a quantitative way, by the large intrinsic quadrupole moment. The concept of shape, shape changes and rotations of shapes at high frequencies will be the subject of the present chapter.

In section 13.1 we shall concentrate on the various manifestations in which the deformed shape, and thus the average field, influences the nuclear single-particle motion. The clearest development is made using the Nilsson potential, which gives rise to all of the salient features characteristic of deformed single-particle motion. It is also pointed out how the total energy of a static, deformed nucleus can be evaluated and that a minimization of this total energy expression will give rise to stable, deformed minima. In section 13.2 we study the effect of rotation on this single-particle motion and discuss the cranking model as a means of providing a microscopic underpinning of the rotational nuclear structure. Finally, in section 13.3, we apply the above description to attempt to understand nuclear rotation at high and very-high spins and the phenomenon of superdeformation as an illustration of these somewhat unexpected, exotic nuclear structure features.

13.1 The harmonic anisotropic oscillator: the Nilsson model

Starting from a spheroidal distribution or deformed oscillatory potential with frequencies ω_x, ω_y and ω_z in the directions x, y, z, the Hamiltonian governing the nuclear single-particle motion becomes

$$H_{\text{def}} = -\frac{\hbar^2}{2m}\Delta + \frac{1}{2}m(\omega_x^2 x^2 + \omega_y^2 y^2 + \omega_z^2 z^2). \tag{13.1}$$

The three frequencies are then chosen to be proportional to the inverse of the half-axis of the spheroid, i.e.

$$\omega_x = \mathring{\omega}\frac{R_0}{a_x}; \ldots, \tag{13.2}$$

with a necessary condition of volume conservation

$$\omega_x\omega_y\omega_z = \mathring{\omega}_0^3. \tag{13.3}$$

This Hamiltonian is separable in the three directions and the energy eigenvalues and eigenfunctions can easily be constructed using the results for the one-dimensional harmonic oscillator model.

For axially symmetric shapes, one can introduce a deformation variable δ, using the following prescription

$$\begin{aligned} \omega_\perp (= \omega_x = \omega_y) &= \omega_0(\delta)(1 + \tfrac{2}{3}\delta)^{1/2} \\ \omega_z &= \omega_0(\delta)(1 - \tfrac{4}{3}\delta)^{1/2} \end{aligned} \tag{13.4}$$

where volume conservation is guaranteed up to second order in δ giving the deformation dependence $\omega_0(\delta)$ as

$$\omega_0(\delta) = \mathring{\omega}_0(1 + \tfrac{2}{3}\delta^2). \tag{13.5}$$

According to Nilsson (1955), one introduces a deformation dependent oscillator length $b(\delta) = (\hbar/m\omega_0(\delta))^{1/2}$ so that dimensionless coordinates, expressed by a prime $\vec{r}', \theta', \varphi', \ldots$, can be used and the Hamiltonian of equation (13.1) now becomes

$$H_{\text{def}} = \hbar\omega_0(\delta)\left(-\frac{1}{2}\Delta' + \frac{r'^2}{2} - \frac{1}{3}\sqrt{\frac{16\pi}{5}}\delta r'^2 Y_{20}(\hat{r}')\right). \tag{13.6}$$

This Hamiltonian reduces to the spherical, isotropic oscillator potential to which a quadrupole deformation or perturbation term has been added. It is clear that this particular term will split the m degeneracy of the spherical solutions (j, m) and the amount of splitting will be described by the magnitude of the 'deformation' variable δ. In the expression (13.6), we can identify the quantity $\frac{1}{3}\sqrt{16\pi/5}\delta$ with the deformation parameter β as used in Chapter 12 (section 12.1).

Since spherical symmetry is broken but axial symmetry remains, the solutions to the Hamiltonian (13.6) can be obtained using cylindrical coordinates with the associated quantum numbers n_z, n_ρ, m_l (with m_l the projection of the orbital angular momentum on the symmetry axis), also called $\Lambda = m_l$.

With the relations $N = n_x + n_y + n_z = n_z + 2n_\rho + m_l$, the eigenvalues become

$$\varepsilon_\delta(N, n_z) \cong \hbar\mathring{\omega}_0\left[(N + 3/2) + \delta\left(\frac{N}{3} - n_z\right)\right], \tag{13.7}$$

which implies a splitting, linear in the number of oscillator quanta in the z direction, as a function of the deformation variable δ.

Including also intrinsic spin, with projection $\Sigma = \pm\frac{1}{2}$, the total projection $\Omega = \Lambda + \Sigma$ of spin on the symmetry axis remains a good quantum number and characterizes the eigenstates in a deformed potential with axial symmetry. The coupling scheme is drawn in figure 13.1(b) as well as the energy splitting of equation (13.7), in a schematic way. One can then characterize a deformed eigenstate with the quantum numbers

$$\Omega^\pi[N, n_z, \Lambda] \tag{13.8}$$

with π the parity of the orbit, defined as $\pi = (-1)^l$.

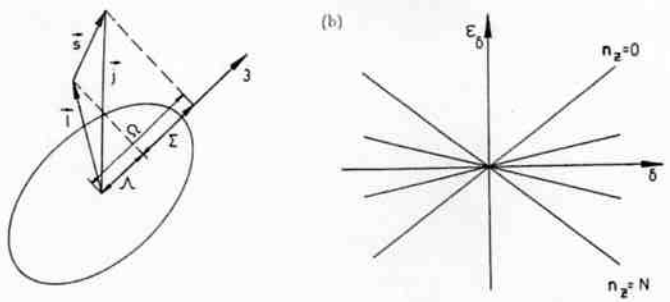

Figure 13.1. (*a*) Coupling scheme indicating the various angular momenta $(\vec{l}, \vec{s})\vec{j}$ and their projection $(\Lambda, \Sigma)\Omega$, on the symmetry axis (3-axis) respective for a particle moving in a deformed, axially symmetric potential. (*b*) Energy levels, corresponding to an anisotropic harmonic oscillator potential, as a function of deformation (δ) and for a varying number of oscillator quanta along the 3-axis, denoted by n_z ($n_z = 0, \ldots, N$).

Large degeneracies remain in the axially symmetric harmonic oscillator if the frequencies $\omega_\perp$ and ω_z are in the ratio of integers, i.e. $\omega_z/\omega_\perp = p/q$. For $p : q = 1 : 1$ one regains the spherical oscillator; for $p : q = 1 : 2$ one obtains 'superdeformed' prolate or, if 2:1, oblate shapes, etc. In figure 13.2, a number of important ratios are indicated on the axis of deformation.

Even though this level scheme contains the major effects relating to nuclear deformation, the strong spin–orbit force needs to be added to transform it to a realistic deformed single-particle spectrum. Moreover, in the original Nilsson parametrization, a $\hat{l}^2$ term has also been added to simulate a potential which appears to be more flat in the nuclear interior region, compared to the oscillator potential. So, the Nilsson Hamiltonian, descibing the potential is

$$H_{\text{Nilsson}} = \hbar\omega_0(\delta)\left(-\frac{1}{2}\Delta' + \frac{r'^2}{2} - \beta r'^2 Y_{20}(\hat{r}')\right) - k\hbar\mathring{\omega}_0(2\hat{l}\cdot\hat{s} + \mu(\hat{l}^2 - \langle\hat{l}^2\rangle_N), \quad (13.9)$$

where 2κ describes the spin-orbit strength and $\kappa\mu$ the $\hat{l}^2$ orbit energy shift. The new terms, however, are no longer diagonal in the basis $|Nn_z, \Lambda\Sigma(\Omega))$, or in the equivalent $|Nlj, \Omega\rangle$ spherical basis. It is also easily shown that $[H_{\text{Nilsson}}, \hat{j}^2] \neq 0$ and only Ω^π are the remaining correct quantum numbers. The Hamiltonian (13.9) has to be diagonalized in a basis. The original Nilsson article considered the basis $|Nn_z\Lambda\Omega\rangle$ to construct the energy matrix. The results for such a calculation for light nuclei is presented in figure 13.3 and is applicable to the deformed nuclei that are situated in the p-shell ($A \simeq 10$) and in the mid-shell s,d region ($A \simeq 26, 28$).

In the region of small deformation, the quadrupole term $\alpha r'^2 Y_{20}(\hat{r}')$ can be used as a perturbation and be evaluated in the basis in which the spin-orbit and $\hat{l}^2$ terms become diagonal i.e. in the $|Nlj, \Omega\rangle$ basis. The matrix element

$$\langle Nlj\Omega|r'^2 Y_{20}(\hat{r}')|Nlj\Omega\rangle \propto \frac{3\Omega^2 - j(j+1)}{(2j-1)(2j+3)} \quad (13.10)$$

is obtained and describes the (Ω, j) dependence near zero deformation.

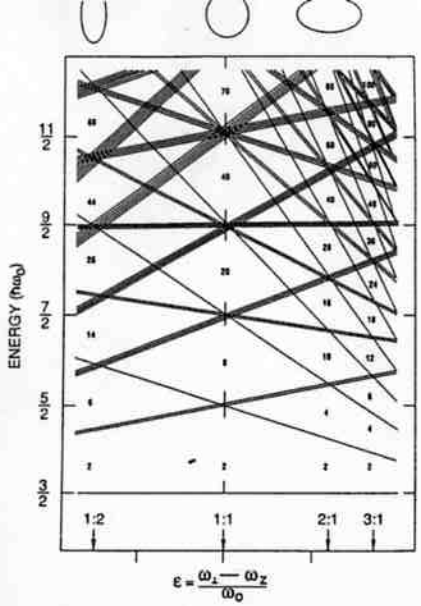

Figure 13.2. Single-particle level spectrum of the axially symmetric harmonic oscillator, as a function of deformation (ε). Here, $\omega_0 = \frac{1}{3}(2\omega_\perp + \omega_z)$. The orbit degeneracy is $n_\perp + 1$ which is illustrated by artificially splitting the lines. The arrows indicate the characteristic deformation corresponding to the ratio of $\omega_\perp/\omega_z = 1/2, 1/1, 2/1$ and $3/1$ (taken from Wood *et al* 1992).

For very large deformations, on the other hand, the $\hat{l}$, $\hat{s}$ and $\hat{l}^2$ term can be neglected relative to the quadrupole deformation effect. In this limit, the quantum numbers of the anisotropic harmonic oscillator become good quantum numbers. They are also called the asymptotic quantum numbers $\Omega^\pi[N, n_z, \Lambda, \Sigma]$ and are discussed in detail by Nilsson (1955).

The original Nilsson potential, with the $r'^2 Y_{20}(\hat{r}')$ quadrupole term has the serious drawback of non-vanishing matrix elements, connecting the major oscillator quantum number N to $N \pm 2$. Using a new coordinate system gives rise to 'stretched' coordinates with a corresponding deformation parameter ε_2 ($\equiv \varepsilon$), the $|\Delta N| = 2$ couplings are diagonalized and form a more convenient basis and representation to study deformed single-particle states. Using a natural extension to deformations, other than just quadrupole, a 'modified' harmonic oscillator potential is given by

$$U_{\text{MHO}} = \tfrac{1}{2}\hbar\omega_0(\varepsilon)\rho_t^2[1 + 2\varepsilon_1 P_1(\cos\theta_t) - \tfrac{2}{3}\varepsilon_2 P_2(\cos\theta_t) + 2\sum_{\lambda=3}^{\lambda_{\max}}\varepsilon_\lambda P_\lambda(\cos\theta_t)] \quad (13.11)$$

where the stretched coordinates ρ_t, θ_t are defined by

$$\cos\theta_t = \cos\theta\left[\frac{1 - \frac{2}{3}\varepsilon_2}{1 + \varepsilon_2(\frac{1}{3} - \cos^2\theta)}\right]^{1/2} \quad (13.12)$$

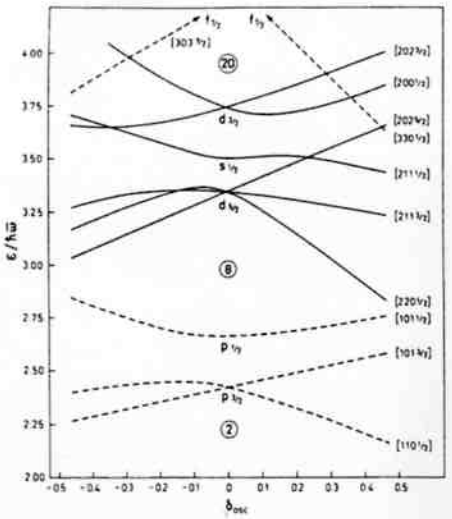

Figure 13.3. Spectrum of a single particle moving in a spheroidal potential ($N, Z < 20$). The spectrum is taken from Mottelson and Nilsson (1959). The orbits are labelled by the asymptotic quantum numbers $[N, n_z, \Lambda, \Omega]$ and refer to prolate deformation. A difference in parity is indicated by the type of lines (full lines: positive parity; dashed lines: negative parity). (Taken from Bohr and Mottelson, *Nuclear Structure*, vol. 2, © 1982 Addison-Wesley Publishing Company. Reprinted by permission.)

and

$$\rho_t^2 = \xi^2 + \eta^2 + \zeta^2 \tag{13.13}$$

with (ξ, η, ζ) the 'stretched' coordinates.

The parameters κ, μ determine the basic that orders and splits the various single-particle orbits and their values are such that at zero deformation the single-particle and single-hole energy spectra are well reproduced. The first evaluation was carried out in the article by Nilsson *et al* but various adjustments, that depend on the specific nuclear mass regions under study, have been carried out.

The Nilsson model has been highly successful in describing a large amount of nuclear data. Even though, at first sight, a Nilsson level scheme can look quite complicated, a number of general features result (see figure 13.4).

(i) Each spherical (n, l, j) level is now split into $j + \frac{1}{2}$ double-generate states, according to the $\pm\Omega$ degeneracy. The Nilsson states are most often still characterized by the $[Nn_z\Lambda\Omega]$ quantum numbers even though these are *not* good quantum numbers, in particular for small deformations.

(ii) According to equation (13.10), orbits with the lower Ω values are shifted downwards for positive (prolate) deformations and upwards for negative (oblate) deformations. This can be understood in a qualitative way by looking at the orientations of these different Ω orbits relative to the z-axis.

(iii) For large deformations we see that levels with the same n_z value are moving in almost parallel lines (see figure 13.4). This peculiar feature is related to a further, underlying symmetry that appears in the deformed shell model (pseudo-spin symmetries).

(iv) Using the spherical basis $|Nlj\Omega\rangle$ to expand the actual Nilsson orbits,

$$|\Omega_i\rangle = \sum c_{lj}^i |Nlj, \Omega\rangle, \tag{13.14}$$

that are near to zero-deformation, the coefficients c_{lj}^i lead to only small admixtures, in particular for the highest (nlj) spherical orbit in each N shell, i.e. $1g_{9/2}$ orbit in the $N = 4$ oscillator shell.

(v) The slope of the Nilsson orbits, characterized by $|\Omega_i\rangle$ and ε_{Ω_i}, is related to the quadrupole single-particle matrix element, or (see equations (13.9) and (13.10))

$$\frac{\mathrm{d}\varepsilon_{\Omega_i}}{\mathrm{d}\beta} = -\hbar\omega_0(\delta)\langle\Omega_i|r'^2 Y_{20}(\hat{r}')|\Omega_i\rangle. \tag{13.15}$$

The matrix elements of the quadrupole operator $r'^2 Y_{20}(\hat{r}')$ have been evaluated using the $|Nlj\Omega\rangle$ basis, and are presented in equation (13.10).

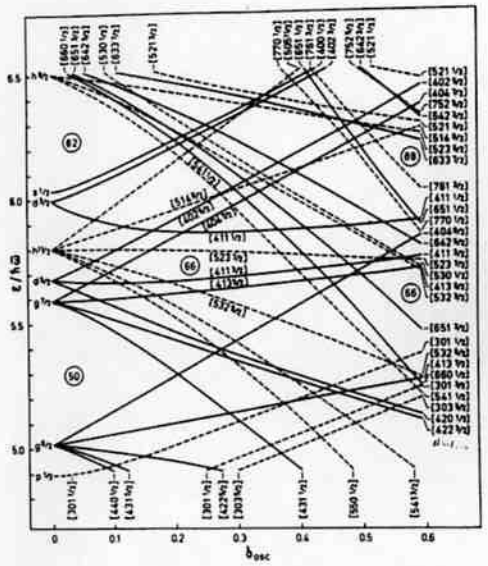

Figure 13.4. As for figure 13.3 but now for $(50 < Z < 82)$. The figure is taken from Gustafson *et al* (1967).

It is now possible to determine the total energy of the nucleus as a function of nuclear deformation. This calculation will allow us to determine the stable, nuclear shapes in a very natural way. At first sight one might think of adding the various deformed single-particle energies; however, one should minimize the total many-body Hamiltonian given by

$$\hat{H} = \sum_{i=1}^{A} t_i + \frac{1}{2}\sum_{i,j} V(i, j). \tag{13.16}$$

The average, one-body field, determined in a self-consistent way by starting from the two-body interaction (Chapter 10), is known to be given by

$$U(i) = \sum_{j=1(j\neq i)}^{A} V(i,j), \tag{13.17}$$

and the full Hamiltonian is be rewritten as

$$\hat{H} = \frac{1}{2}\sum_{i=1}^{A} h_i + \frac{1}{2}\sum_{i=1}^{A} t_i, \tag{13.18}$$

with

$$h_i = t_i + U(i). \tag{13.19}$$

In the case of the oscillator potential $U(i)$ and, because of the well-known virial theorem $\langle t_i\rangle = \langle U_i\rangle = \frac{1}{2}\langle h_i\rangle$, we obtain for the total ground-state energy, if deformation is taken into account

$$E_0(\delta) \equiv \langle\hat{H}\rangle = \frac{3}{4}\sum_{i=1}^{A}\langle h_i\rangle = \frac{3}{4}\sum_{i=1}^{A}\varepsilon_i(\delta) \tag{13.20}$$

where $\varepsilon_i(\delta)$ denotes the eigenvalues of the Nilsson potential. This procedure allows an approximate determination of the ground-state equilibrium values δ_{eq} but absolute values are not so well determined since residual interactions are not well treated in the above procedure. A typical variation of $E_0(\delta)$ as a function of deformation is depicted in figure 13.5 where, besides the total energy, the liquid-drop model variation of the total energy (dashed line) is also presented (Chapter 7).

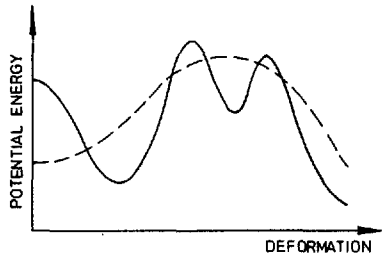

Figure 13.5. Schematic variation of the energy with deformation for a nucleus with a second minimum. The dashed line corresponds to the liquid-drop model barrier.

The basic reason for difficulties in producing the correct total ground-state energy resides in the fact that this property is a bulk property and even small shifts in the single-particle energies can give rise to large errors in the binding energy. To obtain *both* the global (liquid-drop model variations) and local (shell-model effects) variations in the correct way as a function of nuclear deformation, Strutinsky developed a method to combine the best properties of both extreme nuclear model approximations. We do not discuss this Strutinsky procedure (Strutinsky 1967, 1968) which results in adding a shell correction to the liquid-drop model energy

$$E = E_{LDM} + E_{SHELL} \tag{13.21}$$

with

$$E_{SHELL} = \sum_{i=1}^{A}\varepsilon_i(\delta) - \tilde{E}_{SHELL} \tag{13.22}$$

where $\tilde{E}_{SHELL}$ subtracts that part of the total energy already contained in the liquid-drop part E_{LDM}, but leaves the shell-model energy fluctuations. It can be shown that the shell-correction energy is largely correlated to the level density distribution near the Fermi energy. The nucleus is expected to be more strongly bound if the level density is small since nucleons can then occupy more strongly bound single-particle orbits (figure 13.6). As a general rule, in quantum systems, large degeneracies lead to a *reduced* stability. So, a new definition of a magic or closed-shell nucleus is one that is the least degenerate compared to its neighbours. To illustrate the above procedure in more realistic cases, we show in figure 13.7 the E_{SHELL} shell-correction energy, using the modified harmonic oscillator, in which quadrupole, hexadecupole and 6-pole deformations have been included. The presence of the strongly bound (negative E_{SHELL} values) spherical shells at 20, 28, 50, 82, 126 and 184 clearly shows up. Many other deformed shells show up at the same time with the corresponding values of $\varepsilon_2(\varepsilon_4, \varepsilon_6)$ indicated.

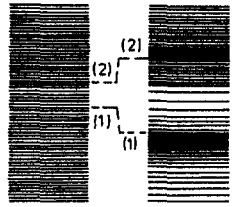

Figure 13.6. Comparison of an equally spaced level density distribution to a schematic shell-model level density. The binding energy of the Fermi level (1), in the right-hand case is stronger than in the left-hand case, whereas for the situation (2), the opposite result is true (taken from Ring and Schuck, 1980).

The above shell-correction description can also be obtained from Hartree–Fock theory (Chapter 10) when the density ρ can be decomposed in a smoothly varying part, ρ_0, and a fluctuating part, $\tilde{\rho}$, that take into account the shell corrections near the Fermi level (Ring and Schuck 1980).

The Strutinsky and/or Hartree–Fock total energy calculations are *the* methods to study ground-state properties (binding energy, deformation at equilibrium shape) in many regions of the nuclear mass table.

13.2 Rotational motion: the cranking model

Up until now, collective rotational motion was considered to be a purely macroscopic feature related to a bulk property of the nucleus. However, nuclear collective motion is built from a microscopic underlying structure which is necessary to determine the collective variables and parameters.

The cranking model allows the inertial parameters to be determined and has many advantages. It provides a fully microscopic description of nuclear rotation; it handles